CONF-880965--2

SAND--88-0628C

OCT 0 C 1988

DE89 000304

THE EFFECT OF DIFFERENT MODULE CONFIGURATIONS ON THE RADIATION TOLERANCE OF MULTIJUNCTION SOLAR CELLS*

James M. Gee
Sandia National Laboratories
Albuquerque, NM 87185

Henry B. Curtis
NASA Lewis Research Center
Cleveland, OH 44135

SUMMARY

The effect of different module configurations on the performance of multijunction (MJ) solar cells in a radiation environment was investigated. Module configuration refers to the electrical circuit in which the subcells of the multijunction cell are wired. Experimental data for AlGaAs, GaAs, InGaAs, and silicon single-junction concentrator cells subjected to 1-MeV electron irradiation was used to calculate the expected performance of AlGaAs/InGaAs, AlGaAs/silicon, GaAs/InGaAs, and GaAs/silicon MJ concentrator cells. These calculations included independent, series, and voltage-matched configurations. The module configuration was found to have a significant impact on the radiation tolerance characteristics of MJ cells.

INTRODUCTION

Multijunction (MJ) solar cells have the potential for extremely high efficiencies (>30%). Such cells consist of several photovoltaically active junctions (subcells) with different bandgaps stacked in optical series. The MJ cell can reach very high efficiencies because it splits the broad solar spectrum into segments to which the individual subcells are better matched. MJ cells are attractive for space applications where high efficiency is important. In order to be useful for space applications, the radiation characteristics of MJ cells need to be examined.

The radiation tolerance of an MJ solar cell is primarily determined by two factors. The first factor is the radiation characteristics of the individual subcells. The degradation characteristics of an individual subcell are typically assumed to be similar, after accounting for shielding by any overlying material, to a single-junction cell fabricated from the same material and with the same cell structure. The radiation tolerance of single-junction solar cells has been extensively studied and documented [1].

The second factor that influences the radiation tolerance characteristics of an MJ cell is its module configuration. Module configuration refers to the electrical circuit in which the subcells of the MJ cell are wired. The degradation characteristics of one subcell may affect the power available from the other subcells through limitations imposed by the electrical circuit. In this paper, we report results of a study concerning the effect of the module configuration on the radiation tolerance of an MJ cell.

* This work was partially supported by the U.S. Department of Energy under contract DE-AC04-76DP00789.

DISCLAIMER

MJ CELL CONFIGURATIONS

The simplest module configuration for an MJ cell has the subcells connected in series. An MJ cell with a series configuration has only two terminals. The current from a series string of solar cells is limited by the cell with the lowest current. The bandgaps of the subcells for a series-configured MJ cell should therefore be chosen for matched photocurrents. The size of a space photovoltaic array is dictated by the power requirements of the satellite at end-of-life (EOL). Hence, the efficiency should be maximized at EOL, so that the bandgaps should be chosen for matched currents at EOL. Since many cells degrade more rapidly in current than in voltage, current matching could impose severe limitations to the EOL efficiency of MJ cells with a series configuration.

MJ cells whose subcells can be wired in various series/parallel circuits have been recently described [2]. The voltage of cells in parallel is limited by the cell with the lowest voltage. Hence, these MJ cells require matched voltages between parallel subcell circuits for efficient operation and are referred to as having a voltage-matched (VM) configuration. An example of two-junction, four-terminal MJ cells wired in a 2x4 VM configuration are given in Figure 1. In a 2x4 circuit, there are 4 strings of 2 series-connected top cells in parallel with 2 strings of 4 series-connected bottom cells. Note that when the subcells are individually contacted, a variety of VM circuits (m x n) could be used, so that a VM circuit could match the voltages of virtually any bandgap combination [3]. Consider, for example, a GaAs/silicon mechanically stacked, multijunction (MSMJ) solar cell. These cells are of interest because the subcells are already highly developed [4,5]. Recently, an efficiency in excess of 30% (350 suns, AM1.5D) has been reported for a GaAs/silicon MSMJ concentrator cell [4]. An appropriate VM configuration for this cell is a 2x3 circuit, which has 3 strings of 2 series-connected GaAs top cells in parallel with 2 strings of 3 series-connected silicon bottom cells. VM circuits have also been described for both two- and three-junction MJ cells with three terminals, so that the VM configuration may be used with monolithic MJ cells [2].

Another module configuration that may be used with MJ cells has all the subcells operated independently. This configuration requires that each subcell have two terminals, be dielectrically isolated, and have independent loads for the subcell circuits. These features make this configuration rather complex and it is probably impractical for space applications; nevertheless, the independent configuration yields the highest efficiency for an MJ cell since each subcell is operated at its individual maximum-power point.

The design of the MJ cell is affected by the module configuration. In particular, selection of bandgaps for an optimized cell has different criteria (matched currents or voltages) for the series and VM configurations. Figures 2 and 3 show the effect of the module configuration on the efficiency versus bandgap relationship for series and VM configurations. (These efficiencies were calculated using the model of Reference 2.) An advantage of the VM configuration compared to the series configuration is that it allows a wider selection of bandgaps for a given efficiency. This allows for a wider selection of materials for the subcells when designing an MJ cell.

EXPERIMENT AND CALCULATIONS

In general, the voltage and current of a solar cell degrade at different rates with irradiation. Hence, the radiation tolerance of an MJ cell is expected to be influenced by the module configuration. While there has been progress with MJ cells, they are not yet available for radiation studies. Also, a general model that can accurately predict the radiation performance of an arbitrary solar cell does not yet exist. For this study, we chose to calculate the performance of several MJ cells using measured data from candidate subcells. This procedure assumes that a cell has the same radiation performance when operated as a single-junction stand-alone solar cell and as a subcell in a MJ stack. We believe this approach to be adequate to access performance variations between different MJ cell configurations.

For this study, we used the measured current-voltage (IV) characteristics of AlGaAs (1.72 eV), GaAs (1.42 eV), InGaAs (1.15 eV), and silicon (1.12 eV) concentrator cells subjected to 1-MeV electron irradiation up to a fluence of $3x10^{15}$ electrons/cm^2. The IV characteristics of these cells were then used to calculate the expected performance of various MJ cells as a function of 1-MeV electron fluence. The MJ cells considered include AlGaAs/silicon, AlGaAs/InGaAs, GaAs/silicon, and GaAs/InGaAs. The first two MJ cells with the AlGaAs top cell have an appropriate bandgap combination for either a series or a 1x2 VM configuration. This bandgap combination is, in fact, nearly ideal for a two-junction MJ cell (Figure 2). The two MJ cells with a GaAs top cell are of interest due to recent progress with GaAs-based MSMJ solar cells. A 2x3 VM configuration was used for these MJ cells. A series configuration was not considered for the GaAs-based MJ cells since this bandgap combination does not have matched photocurrents and would perform very poorly in a series configuration. Performance of MJ cells with an independent configuration was also calculated for all four MJ cells as a base of comparison.

The radiation performance of the AlGaAs, GaAs, InGaAs, and silicon concentrator cells as well as the measurement procedure has been presented previously [6]. The initial device characteristics for these concentrator cells are presented in Table 1. Their performance as a function of 1-MeV electron fluence are presented in Figures 4, 5, 6, and 7. Only the characteristics under concentration (100 suns, AM0) were considered in this paper, since the first application for a high-efficiency MJ cell in space is likely to be a concentrator. Note that the maximum power (P_{max}) of the InGaAs and silicon cells degrade very rapidly due to the rapid degradation of the current.

	AlGaAs	GaAs	InGaAs	Silicon
J_{sc} (A/cm^2)	1.961	3.174	3.579	3.834
V_{oc} (volts)	1.367	1.139	0.859	0.724
Fill Factor	0.835	0.799	0.794	0.800
Efficiency (%)	16.5	21.3	18.1	16.4

Table 1. Initial performance data of the concentrator cells at 100 suns, AM0 and 25°C.

The performance of an MJ cell using the above concentrator cells as the subcells was calculated using the following procedure. Each illuminated IV curve was fitted to a conventional lumped-parameter model consisting of a current source, two diodes (n=1 and n>1), and a shunt and series resistance. No physical interpretation was attached to these fitted parameters; the purpose of this procedure was to allow addition of IV curves for MJ cell modeling. Next, the MJ cell performance for independent, series, and VM configurations (as appropriate) was calculated using the lumped parameter model for the subcells. For the AlGaAs-based MJ cells, the photocurrent of the bottom cell was set equal to the photocurrent of the AlGaAs subcell at beginning-of-life (BOL); i.e. we have assumed that the photocurrents are matched at BOL for an optimized MJ cell. This bandgap combination is, in fact, approximately current matched at BOL. For the GaAs-based MJ cells, the photocurrent at BOL of the InGaAs and silicon bottom cells were set to 5.0 and 7.5 mA/cm^2, respectively. These values are consistent with recent measurements for GaAs-based MSMJ cells [4]. The photocurrents from the InGaAs and silicon cells in the stack were assumed to degrade at the measured rates given in Figures 4 and 6. Note that this data was taken with full spectrum illumination while the bottom cell of a stack will only be illuminated by the spectrum filtered by the top cell.

The BOL and EOL (3E15 1-MeV electrons/cm^2) efficiencies calculated with the above model for the four MJ cells are presented in Table 2. The performance of the MJ cells as a function of fluence are presented in Figures 8 to 11. Given the approximations inherent in our model, the absolute values of the efficiencies (Table 2) are not as significant as the differences in efficiency between different configurations and at different fluence levels. Note that the EOL efficiencies of the VM and independent configurations are nearly the same for all four MJ cells. Note, also, that the difference in efficiency between the VM and independent configurations is indistinguishable in the plots for the AlGaAs/silicon and GaAs/InGaAs MJ cells (Figures 9 and 10).

Cell	Configuration	Efficiency (%)		
		BOL	EOL	Δ
AlGaAs/InGaAs	Ind.	26.50	15.88	0.599
	Series	26.47	11.45	0.433
	1x2 VM	25.81	15.86	0.614
AlGaAs/Si	Ind.	25.30	16.71	0.660
	Series	25.30	14.04	0.555
	1x2 VM	25.30	16.71	0.660
GaAs/InGaAs	Ind.	23.42	15.45	0.660
	2x3 VM	23.42	15.45	0.660
GaAs/Si	Ind.	24.38	16.13	0.662
	2x3 VM	24.08	16.05	0.660

Table 2. Calculated efficiencies at BOL and EOL for the MJ cells at 100 suns, AM0 and 25°C. Ind., Series, and VM refers to independent, series, and voltage-matched configurations, respectively.

DISCUSSION

There are two items regarding results of our calculations that deserve particular attention. The first item to note is that the series-configured MJ cells degrade very rapidly due to the rapid degradation in I_{sc} for the bottom cell. The P_{max} of the series-configured MJ cells, in fact, becomes less than that of a single-junction GaAs cell at high fluences despite the much higher BOL efficiency. Since the top cell produces most of the power from an MJ cell, it is very important that the output of the top cell not be limited by the bottom cell. The bandgaps should be chosen for matched currents at EOL, which requires either AlGaAs with a wider bandgap or a bottom cell with a narrower bandgap. While the EOL P_{max} would be improved with EOL matched currents, it would still be less than that of the independent configuration with the present bandgap combination because the new bandgap combination for EOL current matching would be less optimum (Figure 2).

The second item to note is that the VM configuration performs nearly as well as the independent configuration for all four MJ cells over the entire fluence range. The P_{max} degradation of the VM configuration is much less than that of the series configuration since voltage degrades much less rapidly than current for these particular subcells. The AlGaAs/InGaAs MJ cell is particularly interesting. The VM configuration for this cell initially produces about 3% less power at BOL than the series or independent configurations because the voltages of the subcells are slightly mismatched. However, the subcell voltages become better matched as they degrade with irradiation such that the P_{max} for the VM configuration is nearly the same as for the independent configuration at EOL. Also note that the P_{max} of the VM and independent configurations are about 39% greater than the P_{max} of the series configuration at EOL for the AlGaAs/InGaAs cell. For the AlGaAs/silicon cell, the voltages of the subcells are nearly matched over the entire fluence range, so that the difference in performance between the independent and VM configurations is negligible. Again, both the independent and VM configurations have higher efficiencies than the series configuration at EOL. Similarly, the 2x3 VM configuration for the GaAs-based MJ cells yields an efficiency that is nearly the same as the independent configuration over the entire fluence range.

The superiority of the voltage-matched configuration compared to the series configuration is due to two factors. The first factor is that the voltage degrades less rapidly than the current for these subcells. This is true for a wide variety of solar cells to high-energy particulate radiation. The second factor is that the voltages of the subcells degrade at similar rates while the current degradation varies significantly between different subcells. This implies that a VM-configured MJ cell that is optimized at BOL is still optimal at EOL, while the performance of a series-configured MJ cell is compromised in order to provide EOL current matching.

CONCLUSIONS

We have calculated the expected performance of an AlGaAs/InGaAs, AlGaAs/silicon, GaAs/InGaAs, and GaAs/silicon MJ concentrator cells as a function of 1-MeV electron fluence with series and voltage-matched configurations. It was shown that the module configuration can have a significant impact on the radiation tolerance of an MJ cell due to the

different rates of degradation for voltage and current of the individual subcells. In particular, the VM configuration was found to be superior to the series configuration and to perform nearly as well as the independent configuration for all MJ cells and radiation fluences considered.

ACKNOWLEDGEMENTS

We would like to thank L.D. Partain and D.L. King for many useful discussions regarding MJ cells and D E. Arvizu and D.J. Flood for their support.

REFERENCES

1. See, for example, H. Y. Tada, et al., Solar Cell Radiation Handbook, 3rd Ed., JPL Publication No. 82-69 (November 1982), and other papers in this conference.

2. James M. Gee, "Voltage-matched configurations for multijunction solar cells," Proc. 19th IEEE Photo. Spec. Conf., pg. 536 (1987).

3. L.D. Partain, et al., "High efficiency mechanical stack using a GaAsP cell on a transparent GaP wafer," Proc. 18th IEEE Photo. Spec. Conf., pg. 539 (1987).

4. J.M. Gee et al., "A 31%-efficient GaAs/silicon mechanically stacked, multijunction solar cell," to be published in Proc. 20th IEEE Photo. Spec. Conf., Las Vegas, NV (Sept. 26-30, 1988).

5. L. Bertotti et al., "Large area GaAs/Si mechanically stacked, multijunction solar cells optimized for space application," Proc. 19th IEEE Photo. Spec. Conf., pg. 1512 (1987)

6. H.B. Curtis, C.K. Swartz, and R.E. Hart, Jr., "Radiation performance of AlGaAs and InGaAs concentrator cells and expected performance of cascade structures," Proc. 19th IEEE Photo. Spec. Conf., pg. 727 (1987).

Figure 1. A 2x4 voltage-matched circuit for a four-terminal, two-junction MJ cell [3]. In the above circuit, 4 strings of 2 series-connected top subcells are wired in parallel with 2 strings of 4 series-connected bottom subcells.

Figure 2. Iso-efficiency curves for a two-junction MJ cell as a function of top and bottom subcell bandgaps (1 sun, AM0). The VM configuration is for a 1x2 circuit.

Figure 3. Iso-efficiency curves for a three-junction MJ cell as a function of top and middle subcell bandgaps (1 sun, AM0). For each pair of top and middle subcell bandgaps, the efficiency was calculated with the bandgap of the bottom subcell optimized. For the VM configuration, the top subcell is wired in parallel with the series-connected middle and bottom subcells [2].

Figure 4. Ratio of degraded/initial values for V_{oc}, I_{sc}, and P_{max} of an AlGaAs (1.72 eV) concentrator cell as a function of 1-MeV electron fluence (100 suns, AM0, 25°C).

Figure 5. Ratio of degraded/initial values for V_{oc}, I_{sc}, and P_{max} of a GaAs (1.42 eV) concentrator cell as a function of 1-MeV electron fluence (100 suns, AM0, 25°C).

Figure 6. Ratio of degraded/initial values for V_{oc}, I_{sc}, and P_{max} of an InGaAs (1.15 eV) concentrator cell as a function of 1-MeV electron fluence (100 suns, AM0, 25°C).

Figure 7. Ratio of degraded/initial values for V_{oc}, I_{sc}, and P_{max} of a silicon (1.12 eV) concentrator cell as a function of 1-MeV electron fluence (100 suns, AM0, 25°C).

Figure 8. P_{max} as a function of 1-MeV electron fluence for a GaAs concentrator cell and an AlGaAs/InGaAs MJ concentrator cell with a series, an independent, and a VM configuration (100 suns, AM0, 25°C). P_{max} is normalized with respect to the initial P_{max} of the AlGaAs/InGaAs MJ cell with an independent configuration.

Figure 9. P_{max} as a function of 1-MeV electron fluence for a GaAs concentrator cell and an AlGaAs/silicon MJ concentrator cell with a series, an independent, and a VM configuration (100 suns, AM0, 25°C). P_{max} is normalized with respect to the initial P_{max} of the AlGaAs/silicon MJ cell with an independent configuration.

Figure 10. P_{max} as a function of 1-MeV electron fluence for a GaAs concentrator cell and a GaAs/InGaAs MJ concentrator cell with an independent and a 2x3 VM configuration (100 suns, AM0, 25°C). P_{max} is normalized with respect to the initial P_{max} of the GaAs/InGaAs MJ cell with an independent configuration.

Figure 11. P_{max} as a function of 1-MeV electron fluence for a GaAs concentrator cell and a GaAs/silicon MJ concentrator cell with an independent and a 2x3 VM configuration (100 suns, AM0, 25°C). P_{max} is normalized with respect to the initial P_{max} of the GaAs/silicon MJ cell with an independent configuration.

Fig 1

Module Wiring Diagram

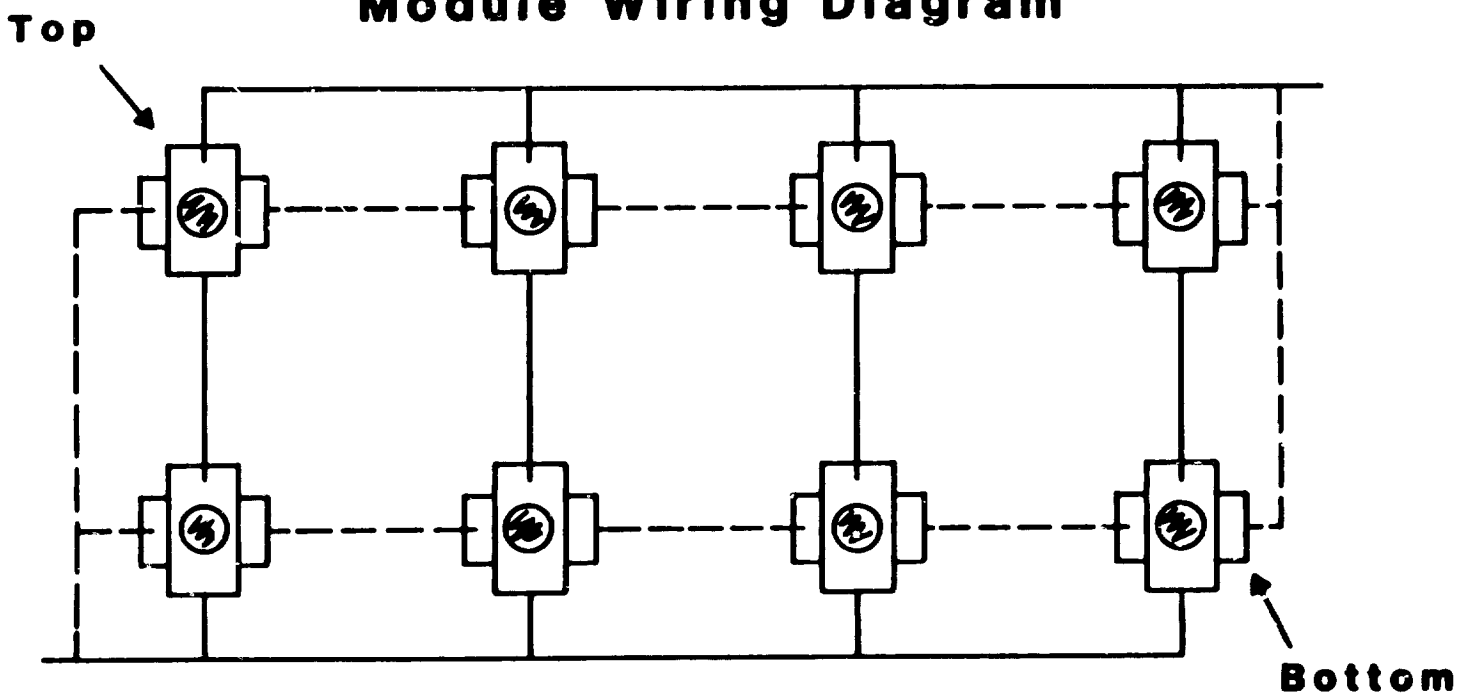

2x4

Fig 2

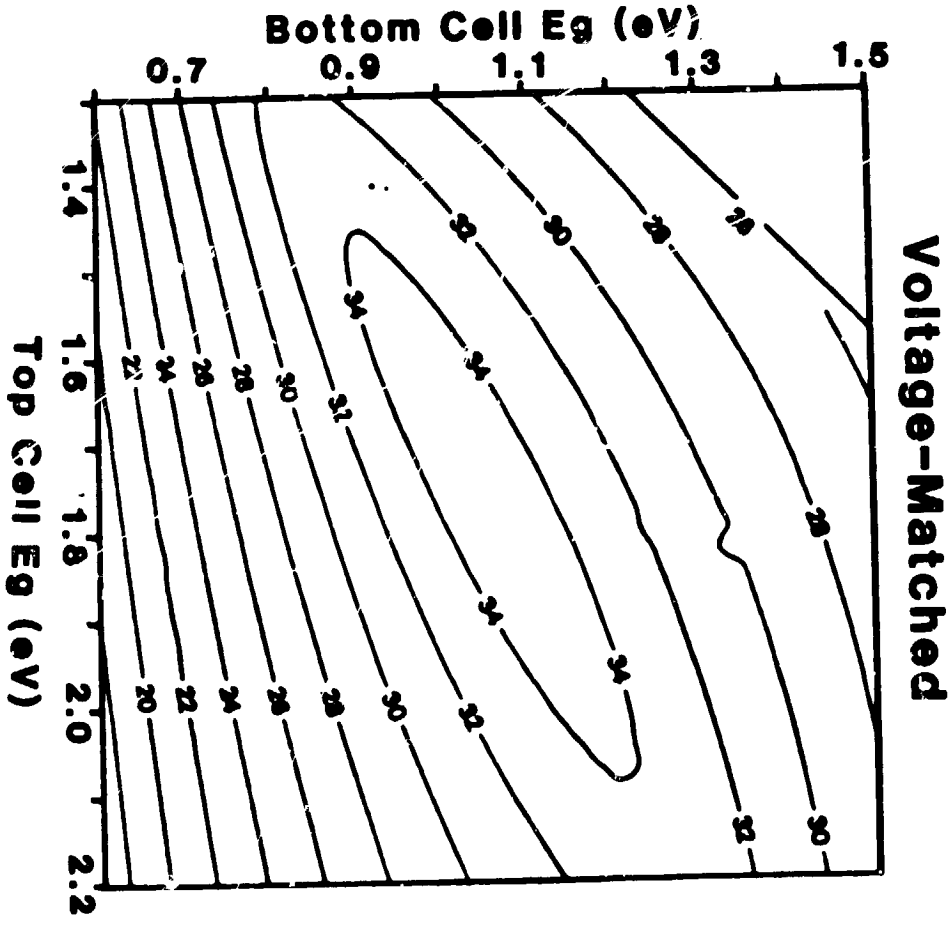

VM AM0

2-jcn

Fig 2

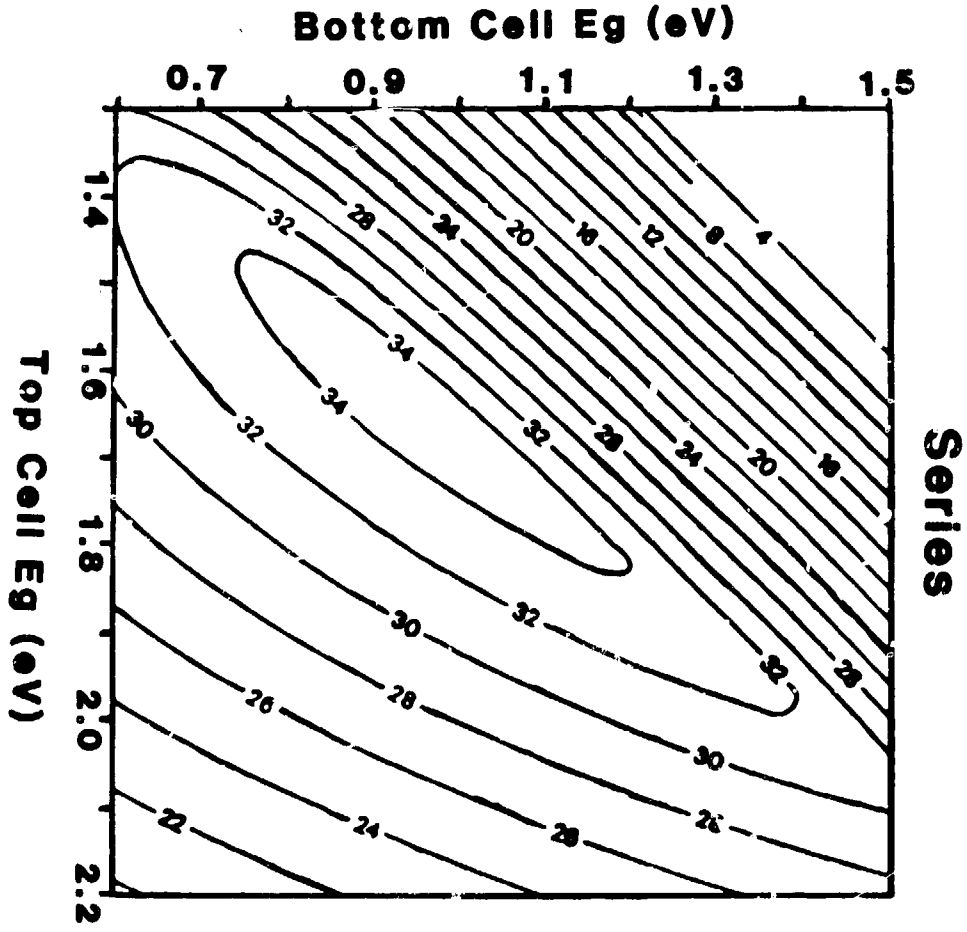

Series AMΦ
2 JCN

Fig 3

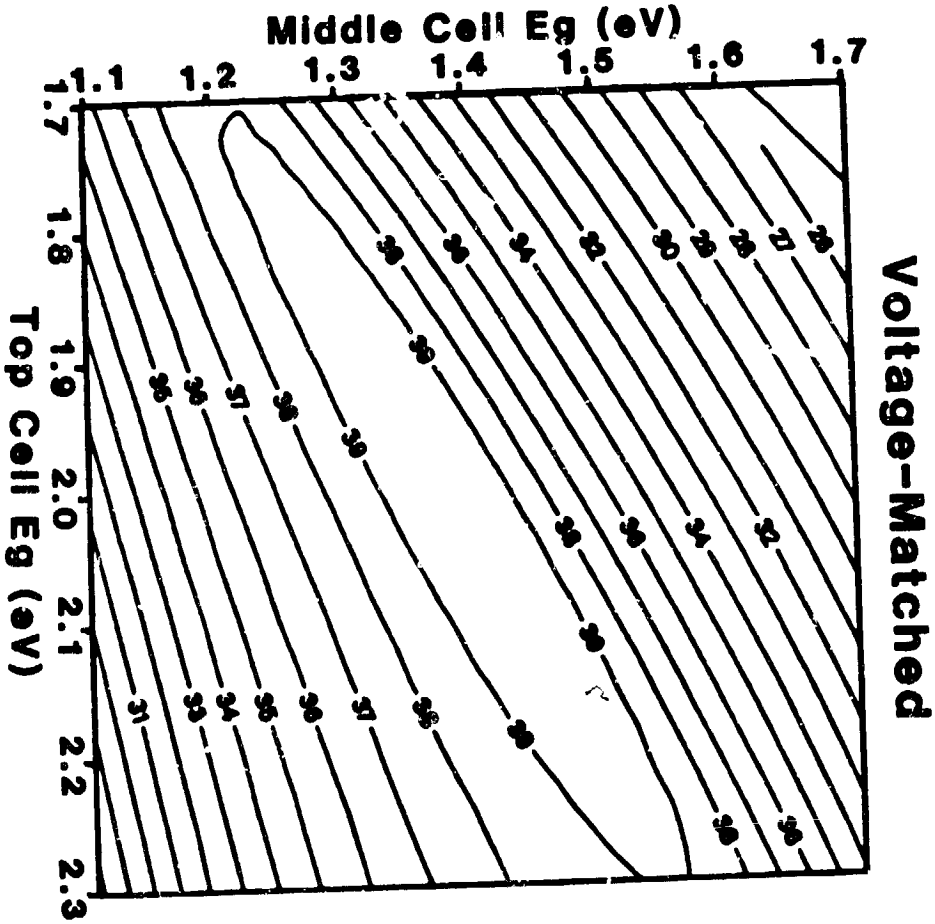

3J VM

AM Ø

Bottom Eg optimized

Fig 3

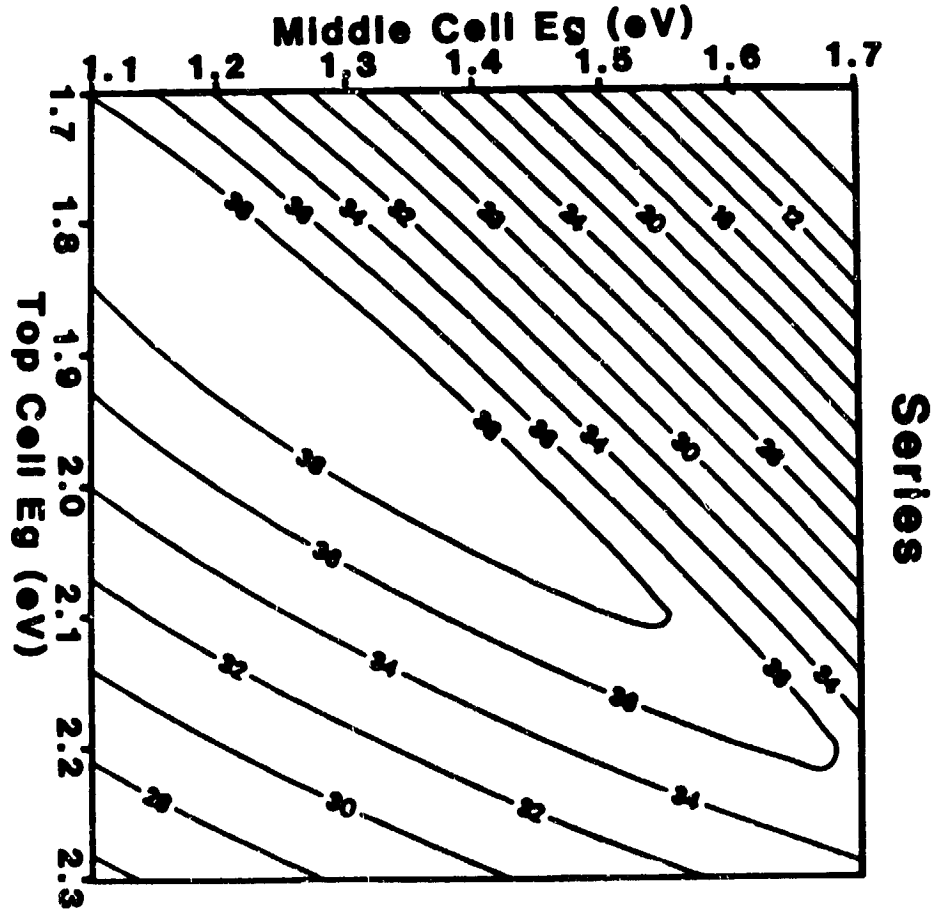

3J Series

AM0

Bottom Eg optimized

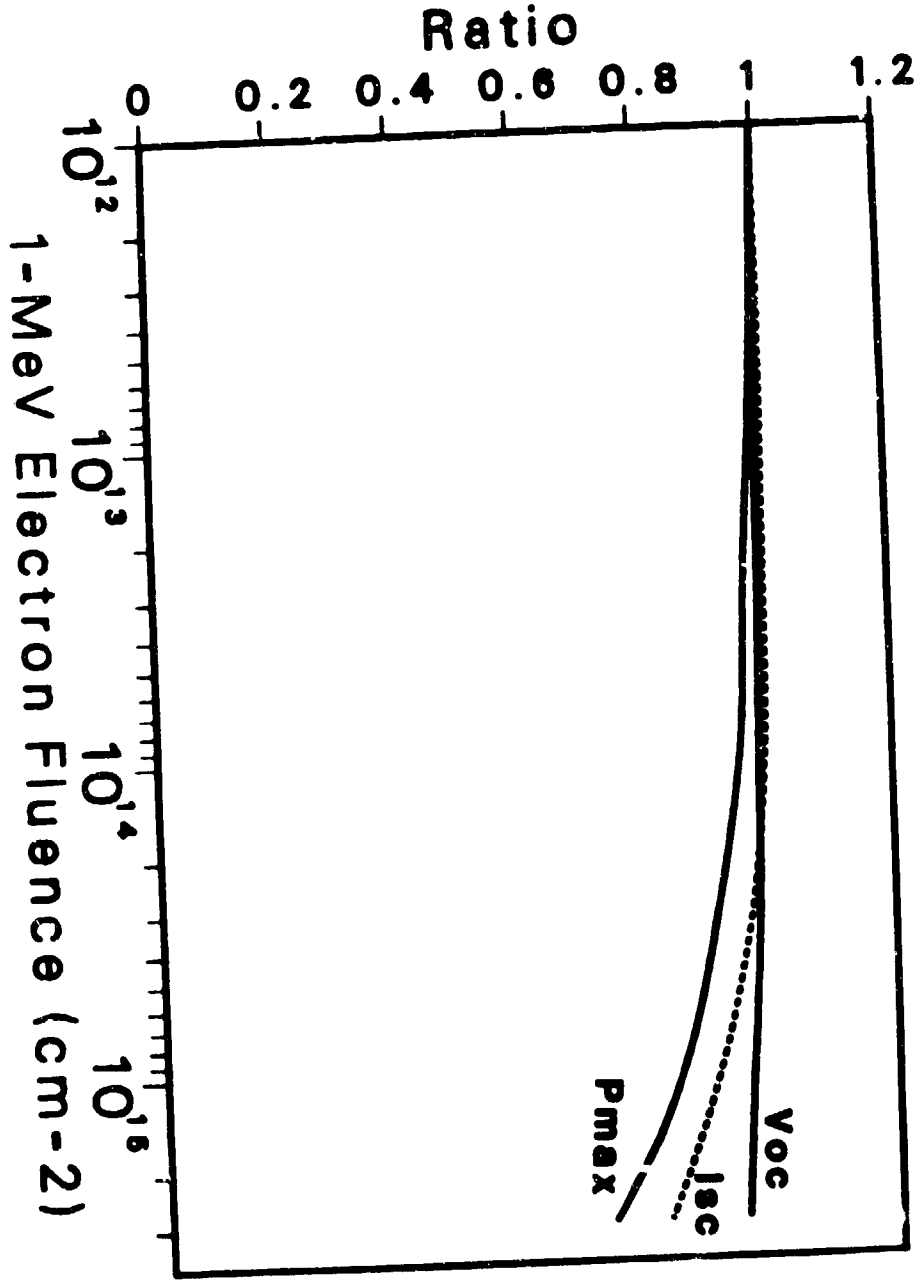
Ratio
0
0.2
0.4
0.6
0.8
1
1.2
1-MeV Electron Fluence (cm-2)
10¹²
10¹³
10¹⁴
10¹⁵
Pmax
Isc
Voc

Fig 5

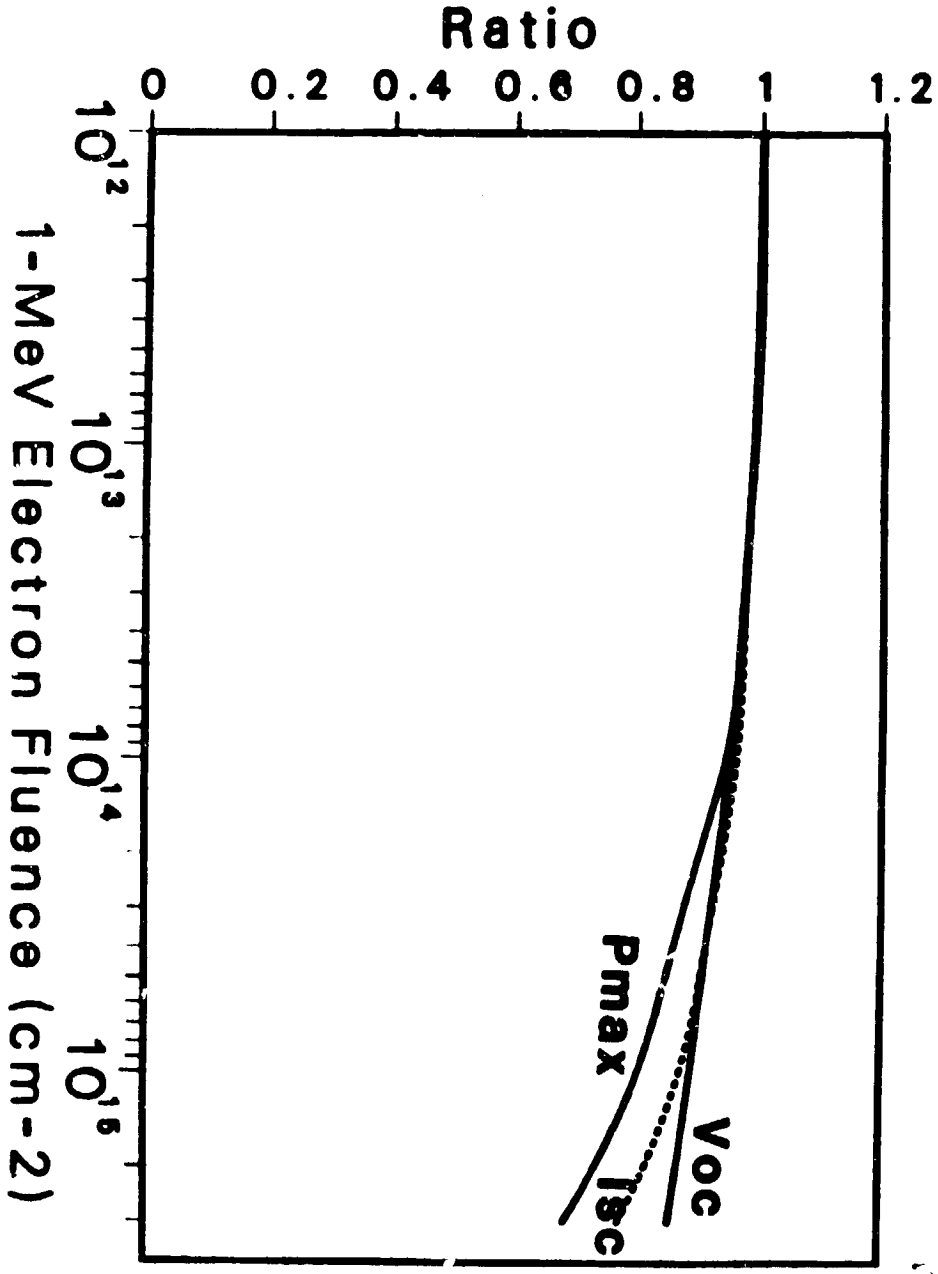
Ratio
0
0.2
0.4
0.6
0.8
1
1.2
1-MeV Electron Fluence (cm-2)
10^12
10^13
10^14
10^15
Pmax
Isc
Voc

Fig 6

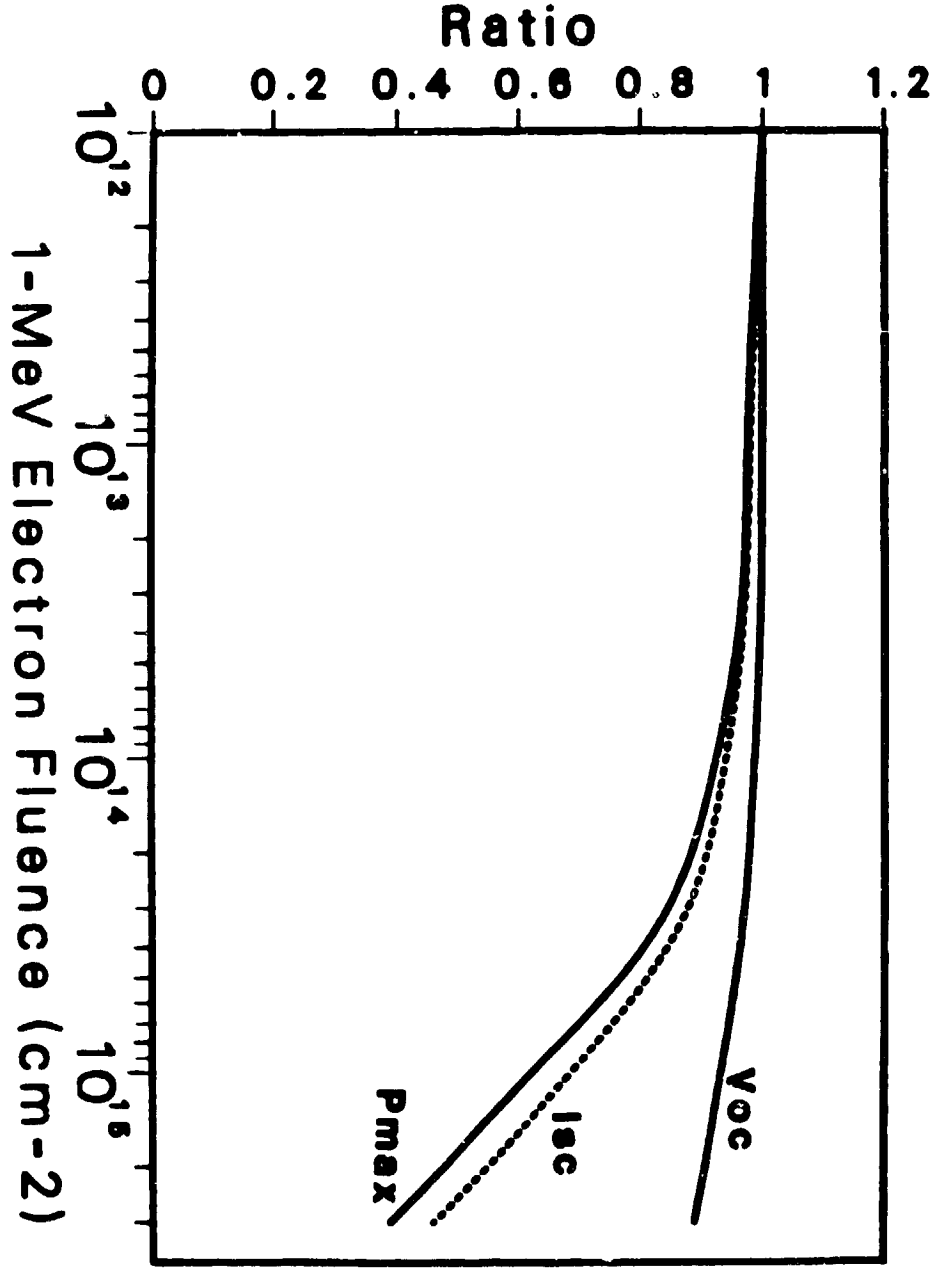
Ratio
0
0.2
0.4
0.6
0.8
1
1.2
1-MeV Electron Fluence (cm-2)
10^12
10^13
10^14
10^15
Pmax
Isc
Voc

Fig 7

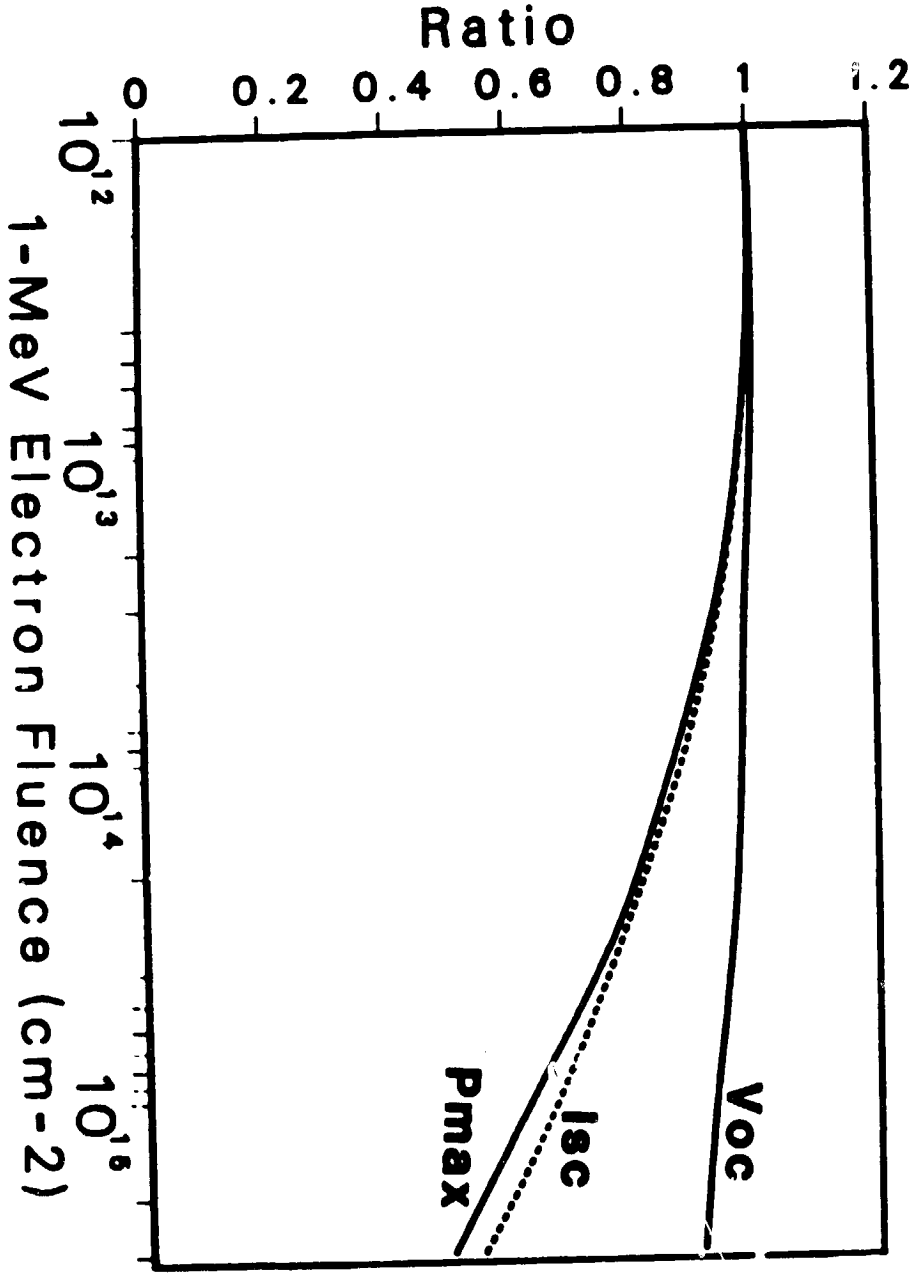
Ratio
0
0.2
0.4
0.6
0.8
1
1.2
1-MeV Electron Fluence (cm-2)
10¹²
10¹³
10¹⁴
10¹⁵
Pmax
Isc
Voc

Fig 8

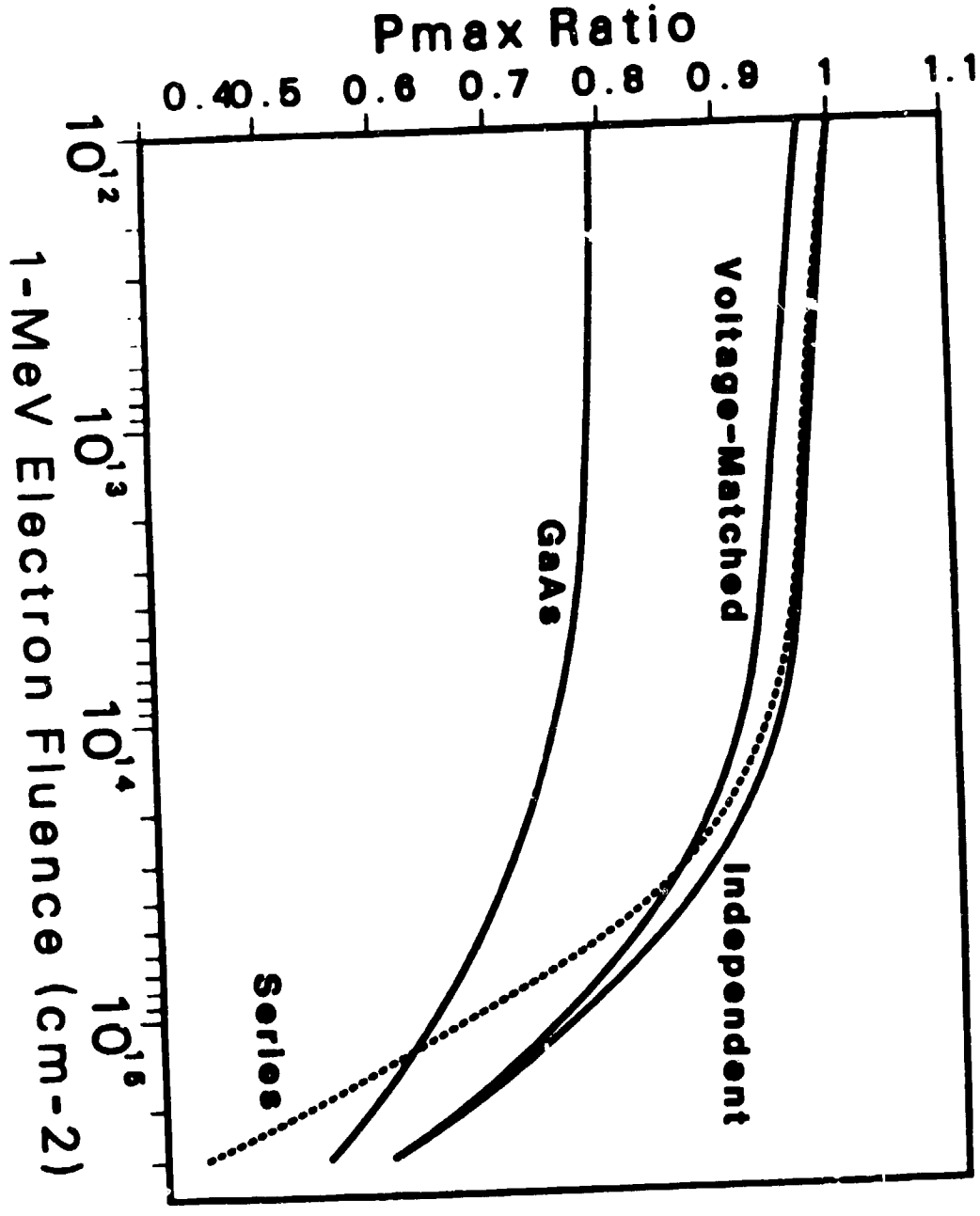
Pmax Ratio
0.4
0.5
0.6
0.7
0.8
0.9
1
1.1
10^{12}
10^{13}
10^{14}
10^{15}
1-MeV Electron Fluence (cm-2)
GaAs
Voltage-Matched
Indopendent
Series

Fig 9

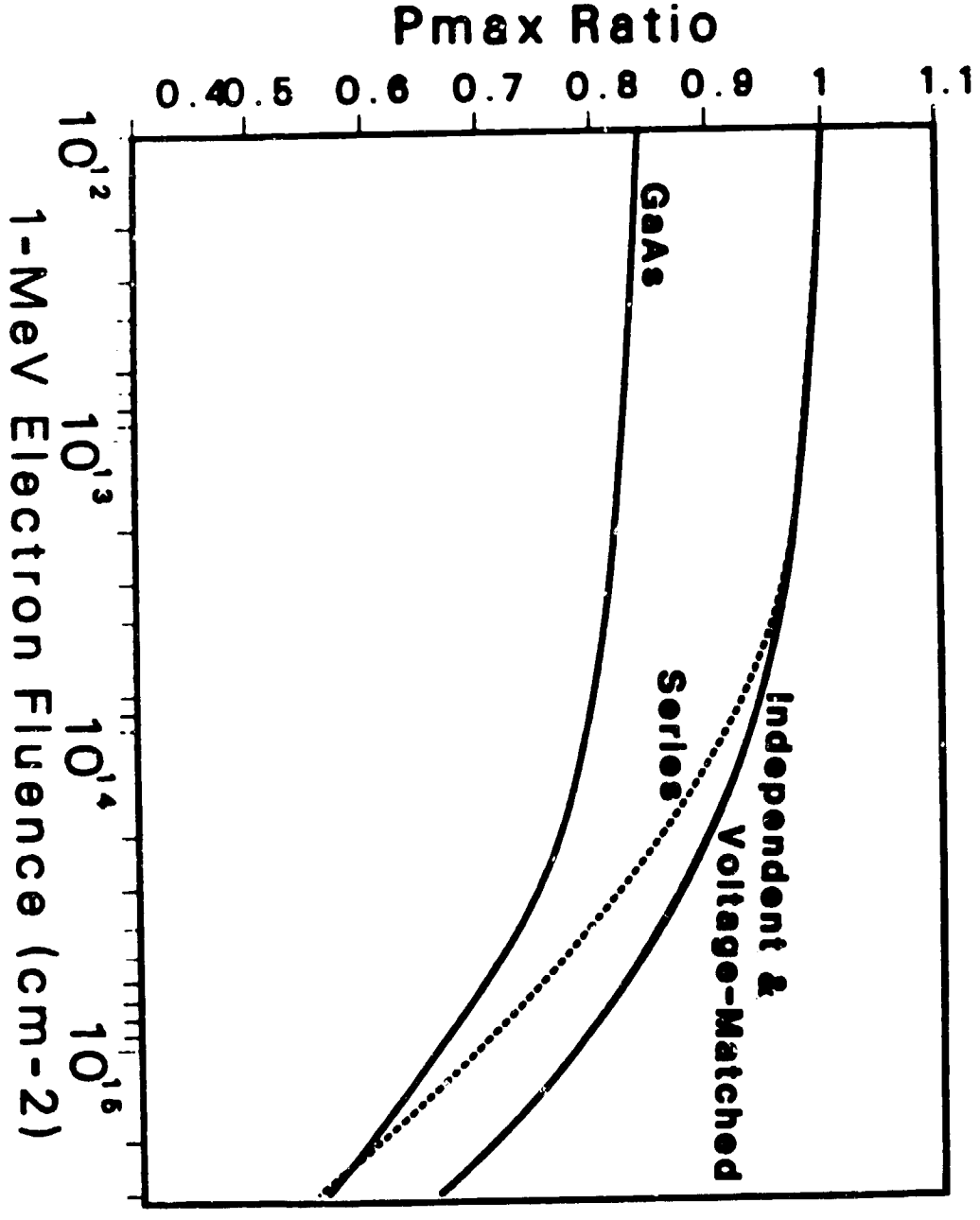

25.3% BOL
AlGaAs/GaAs
Tandem Cell

100x, AMO, 25°C

Ind, Series, &

Fig 10

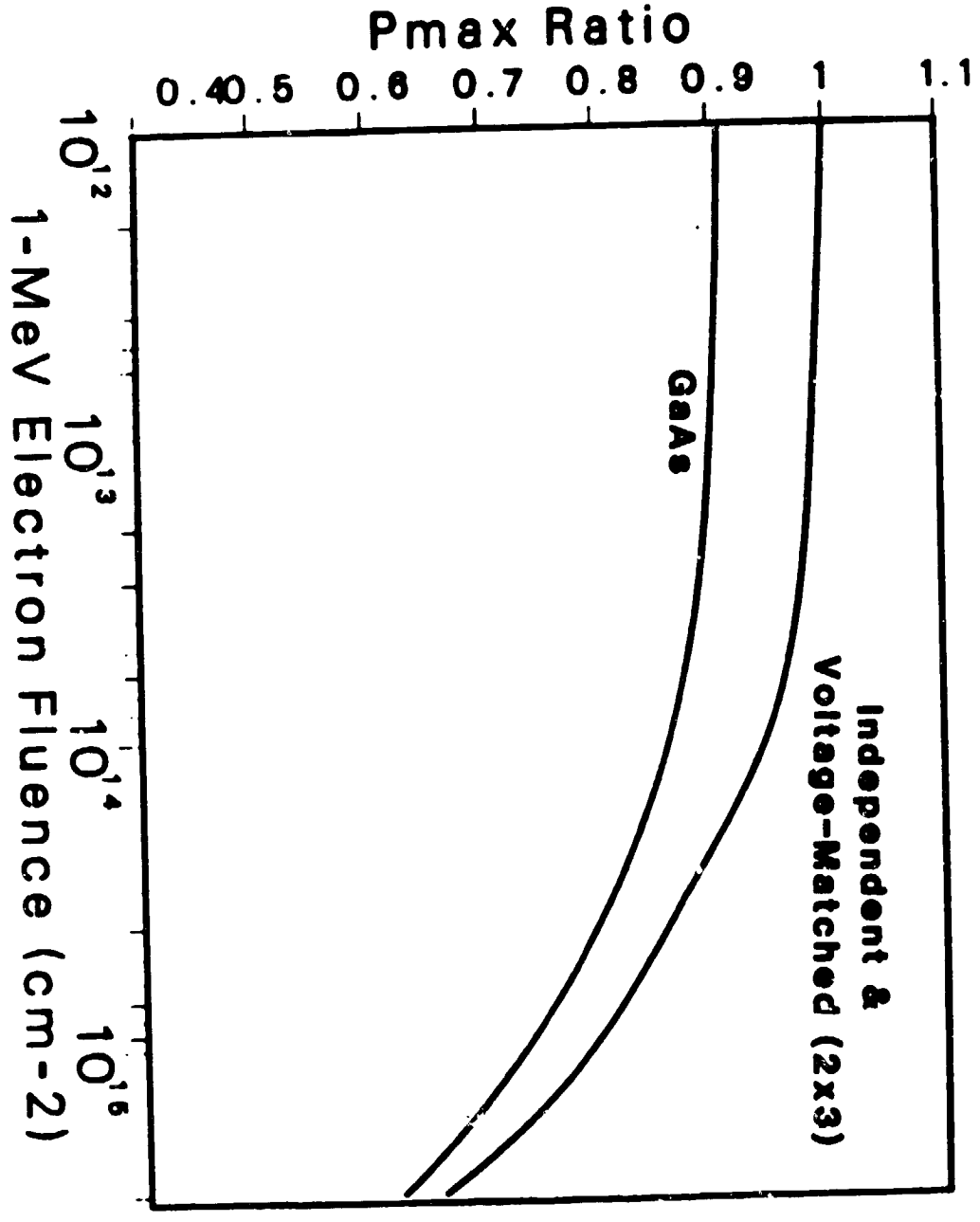
Pmax Ratio
0.4
0.5
0.6
0.7
0.8
0.9
1
1.1
1-MeV Electron Fluence (cm-2)
10^12
10^13
10^14
10^15
GaAs
Independent &
Voltage-Matched (2x3)

Fig 11

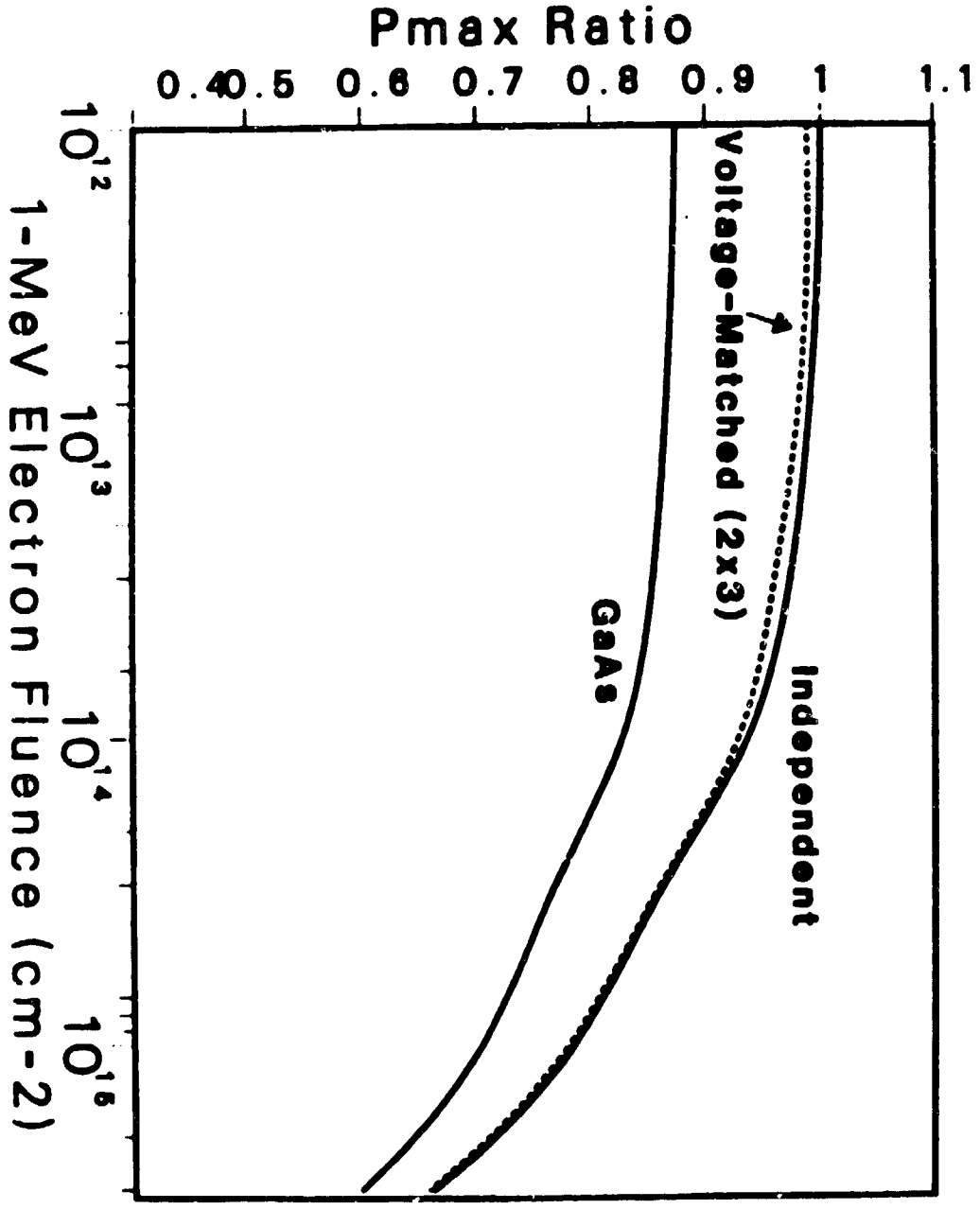
Pmax Ratio
0.4
0.5
0.6
0.7
0.8
0.9
1
1.1
10^{12}
10^{13}
10^{14}
10^{15}
1-MeV Electron Fluence (cm-2)
Voltage-Matched (2x3)
GaAs
Independent

UNCLASSIFIED
SECURITY CLASSIFICATION OF THIS PAGE

ADA197988

REPORT DOCUMENTATION PAGE

Form Approved
OMB No. 0704-0188

1a. REPORT SECURITY CLASSIFICATION Unclassified	1b. RESTRICTIVE MARKINGS
2a. SECURITY CLASSIFICATION AUTHORITY	3. DISTRIBUTION/AVAILABILITY OF REPORT Approved for public release; distribution is unlimited.
2b. DECLASSIFICATION/DOWNGRADING SCHEDULE	
4. PERFORMING ORGANIZATION REPORT NUMBER(S) AAMRL-TR-88-015	5. MONITORING ORGANIZATION REPORT NUMBER(S)
6a. NAME OF PERFORMING ORGANIZATION HARRY G. ARMSTRONG AEROSPACE MEDICAL RESEARCH LABORATORY 6b. OFFICE SYMBOL (If applicable) AAMRL/BBS	7a. NAME OF MONITORING ORGANIZATION AAMRL/BBS
6c. ADDRESS (City, State, and ZIP Code) Wright-Patterson AFB, OH 45433-6573	7b. ADDRESS (City, State, and ZIP Code) Wright-Patterson AFB, OH 45433-6573
8a. NAME OF FUNDING/SPONSORING ORGANIZATION N/A 8b. OFFICE SYMBOL (If applicable)	9. PROCUREMENT INSTRUMENT IDENTIFICATION NUMBER
8c. ADDRESS (City, State, and ZIP Code)	10. SOURCE OF FUNDING NUMBERS PROGRAM ELEMENT NO: 62202F; PROJECT NO: 7231; TASK NO: 35; WORK UNIT ACCESSION NO: 01

11. TITLE (Include Security Classification)
Body Displacement Measured During Sustained +Gz, -Gz, and ±Gy Acceleration Using A Stereoscopic Photographic System (Unclassified)

12. PERSONAL AUTHOR(S)
John Frazier, Joe McDaniel, Vance Skowronski, Nilss Aume, & Donald Stewart*

13a. TYPE OF REPORT	13b. TIME COVERED	14. DATE OF REPORT (Year, Month, Day)	15. PAGE COUNT
Final	FROM Jun 82 TO May 83	March 1988	16

16. SUPPLEMENTARY NOTATION
*Johnson Space Center, Houston, TX

17. COSATI CODES			18. SUBJECT TERMS (Continue on reverse if necessary and identify by block number)
FIELD	GROUP	SUB-GROUP	Acceleration Restraints Body Displacement 07-03
20	11		
05	06		

19. ABSTRACT (Continue on reverse if necessary and identify by block number)

Pilot performance may be adversely affected by G-induced body displacement. Controls may be difficult to reach and activate. The use of a head-up-display may be rendered ineffective by excessive head movement. Also, measurement of body displacement can be useful in evaluating restraint systems. A technique has been devised to quantify body displacement during acceleration studies conducted on the Dynamic Environment Simulator (DES), a three axis centrifuge A stereoscopic photographic system consisting of two motorized 35 mm SLR cameras, a microprocessor controller, and displays were used. Reference marks defining the DES cab in 3 dimensions (3-D) and targets on the subject are recorded photographically. The film strips were then processed on an x-y plotter to digitize the target information. From these data, calculations were performed to compute the 3-D coordinates of the points of interest. Data collected when using the stereoscopic photographic systems are presented on eye and shoulder displacements during various acceleration and restraint conditions. Eye displacements of 3.95 cm at +4.0 Gz, 4.79 cm at -1.0 Gz, and 10.16 cm at 2 Gy are reported. Improving the

20. DISTRIBUTION/AVAILABILITY OF ABSTRACT ☑ UNCLASSIFIED/UNLIMITED ☐ SAME AS RPT ☐ DTIC USERS	21. ABSTRACT SECURITY CLASSIFICATION Unclassified
22a. NAME OF RESPONSIBLE INDIVIDUAL John Frazier	22b. TELEPHONE (Include Area Code) 513-255-2639 22c. OFFICE SYMBOL AAMRL/BBS

DD Form 1473, JUN 86 *Previous editions are obsolete*

SECURITY CLASSIFICATION OF THIS PAGE
UNCLASSIFIED

Block 19 continued:

restraint system by adding lateral shoulder supports reduced the eye displacement at 2 Gy to 3.96 cm (61%). The average lateral restraining force exerted on the shoulder pads at 2 Gy was 55.8 Kg (123 lbs).

PREFACE AND ACKNOWLEDGMENTS

This report documents an in-house experiment conducted on the Dynamic Environment Simulator (DES) at the Acceleration Effects Branch, Biodynamics and Bioengineering Division, Armstrong Aerospace Medical Research Laboratory, Wright-Patterson Air Force Base, Ohio. The effort was conducted under work unit 72313501 in cooperation with AAMRL/HEG. The photographic system described in the report was developed under contract by the University of Dayton Research Institute, Dayton, Ohio. The authors extend their appreciation to Diana Coddington and Vanessa Deer for typing the manuscript and to Van Thai for his assistance with the mathematical equations and computer solutions.

TABLE OF CONTENTS

LIST OF TABLES

LIST OF ILLUSTRATIONS

INTRODUCTION

Pilots of high performance aircraft require a wide variety of body restraint conditions. During most flight conditions the crewmembers desire a high level of mobility in order to activate controls, reach switches, and check rear vision. During some flight environments, however, such as buffet, outside loops, or out-of-control conditions a high level of restraint is necessary. Pilot performance may be degraded by involuntary G-induced body displacement in the cockpit. The forces generated by these types of flight maneuvers may significantly decrease the pilot's ability to control the aircraft or even initiate ejection procedures. Pilots have reported contacting the canopy during -Gz maneuvers (4). Centrifuge studies with human subjects using typical military restraints have been conducted and measurements of 3.8 cm displacement off the seat pan (4) and 12 cm of helmet rise at -2.0 Gz have been documented (5). The measurement of displacement can be a useful quantitative tool in evaluating restraint systems. The use of a head-up-display (HUD) may be rendered ineffective by lateral or vertical head motion of greater than 12.7 cm. A data base relating head and eye positions to acceleration levels would be helpful to cockpit designers. This report describes a photographic system that has been used to measure body displacement on the Dynamic Environment Simulator (DES), a three axis man-rated centrifuge located at Wright-Patterson AFB, OH. Data from various acceleration environments are also presented.

METHODS

Photographic System

A stereoscopic photographic system consisting of two motorized 35 mm single lens reflex (SLR) cameras, two light emitting diode (LED) digital display units, three accelerometers, and a microprocessor controller was used. The cameras (Canon A-1 with 50 mm lens) were mounted in the DES cab in the horizontal plane with a separation angle of approximately 90°. The field of view of each camera included the subject's head, upper torso, and a digital display unit containing X,Y, and Z accelerometer values, film frame counter, date, and subject's name. Reference targets were installed to define the geometry of the DES cab. A minimum of eight targets was used, three of which were required to be in the field of view of both cameras. Also, targets to track body displacement were placed on the subjects. Typical target placements included the shoulders and helmet. The eyes were also used as targets. A subject in the DES cab and reference targets are shown in Figure 1. Figure 2 presents a block diagram and picture of the photographic system. The system can be operated in either an automatic or manual mode. In the automatic mode the microprocessor is programmed to activate the cameras with each acceleration level change of ±0.5 Gx, 0.5 Gy, or 1.0 Gz. The cameras may also be operated manually by personnel in the monitoring room. ASA 400 color slide film was used in this application. The light level in the DES cab was sufficient so that no additional flash lighting was required. The exposed film was processed and left in strip form.

Digitizer

Each target location was manually measured using an X,Y filmstrip digitizer. This unit consists of a 35 mm projector, 50.8 x 50.8 cm rear projection screen, movable X,Y cursor, keyboard, and a paper tape punch unit. As each frame is projected onto the viewing screen, the movable cursor is positioned over each reference target and points of interest on the subject. The vertical (X) and horizontal (Y) coordinates of each location are then punched on eight channel, one inch paper tape. The subject number, date, film frame number, and X,Y, and Z acceleration levels were entered via the keyboard. After the filmstrip data have been encoded onto paper tape, it is transferred to a 9-track magnetic tape for computer processing. An analysis program reads the horizontal and vertical coordinates and computes the 3-D coordinates (X,Y,Z) of the points of interest. Measurement errors with the systems were found to be less than 3%.

RESULTS

Filmstrips have been taken to provide body displacement data during several experiments conducted on the DFS. The primary objectives of those experiments were to measure performance or physiological parameters and are reported separately by others. The displacement measurements quantified by the photographic system are documented in this report.

Experimental setup 1 consisted of a modified Stencel aircraft seat with adjustable lap belt and double shoulder straps (4.4 cm wide). The seat back angle (SBA) was 30° from the vertical. Experiments using this setup are reported by Frazier (1), Guthrie (2), Popplow (6), Repperger (7), and Van Patten (9). Results from this setup are reported in Table I.

TABLE I - DISPLACEMENT DATA COMPILED BY GUTHRIE (2)

	Displacement (cm)		
G	Eye	Helmet	N
-1 Gz	4.79	5.84	12
+1 Gz	0	0	12
+2 Gz	2.43	2.85	12
+3 Gz	2.04	2.67	12
+4 Gz	3.04	3.43	12
+5 Gz	3.43	3.87	12
-2 Gy	7.16	9.19	6
-1 Gy	3.48	4.83	12
+1 Gy	4.87	6.12	12
+2 Gy	6.61	8.45	6

Restraining forces during +Gv acceleration have been measured by instrumenting the left shoulder pad support with a load cell (1). Additional data were subsequently collected by also installing an instrumented head support (Fig. 3). The data are presented in Table II.

TABLE II - LATERAL FORCES (KILOGRAMS)

Gy	Gz	Shoulder Pad (kg) Mean ± s.d.	Helmet Pad (kg)	N
1.0	0	28.6 ± 9.0	--	8
1.5	1.0	37.6 ± 8.6	--	8
1.5	2.0	30.4 ± 9.0	--	8
2.0	1.0	55.8 ± 12.7	--	8
2.0	2.0	47.2 ± 14.5	--	8
2.5	1.0	66.2 ± 18.1	--	8
2.5	2.0	60.4 ± 11.8	--	8
1.5	1.0	33.0	9.0	4
1.5	3.0	28.5	7.0	4
1.5	5.0	27.8	8.1	4
2.0	1.0	44.8	12.1	4
2.0	5.0	32.6	11.4	4

Experimental setup 2 consisted of a rebuilt ACES II seat, SBA of 30°, lap belt, and PCU-15/P torso harness with the inertia reel locked (Figure 4). Additional lateral support was provided by shoulder pads during half of the runs. The shoulder pads were 10 cm x 15.2 cm and were individually adjusted for each subject to provide lateral support at the upper humerus. They were padded with high density foam rubber (1.9 cm thick). The performance and physiological results are reported by Stewart (8). The displacement data are reported in Table III.

TABLE III - DISPLACEMENT DATA IN THE ACES II SEAT

	Mean Displacement (cm) ± Standard Deviation			
	Standard Restraint		Shoulder Pads	
	Eye	Shoulder	Eye	Shoulder
2 Gy	10.16 ±3.55	9.05 ±2.29	3.96 ±1.96	4.08 ±0.40
4 Gz	3.95 ±2.30	1.70 ±0.77	----	----

Displacements at Gy are in the lateral axis and in the vertical axis for Gz.

DISCUSSION

+Gz Acceleration

The acceleration environment most commonly encountered by the aircrew member is in the +Gz direction. In our experiments the highest G levels were attained and the least eye displacement occurred during +Gz. The seat provides good support in this direction. Compression of the seat pan cushion and subject's spinal column and torso would constitute components contributing to eye displacement during +Gz. During these studies the subjects were instructed and able to maintain an upright posture. It is possible, however, during high Gz maneuvers for a crewmember to become slumped over and unable to regain an upright position until the G force is decreased. The initial slumping could occur voluntarily or be induced by factors such as asymmetrical helmet loading or off-axis G force components.

The data by Guthrie (2) records an average eye displacement of 3.43 cm at 5 Gz (Table 1 & Figure 5). At 2.0 Gz, 70% of that displacement was reached, perhaps as the initial compression of the torso and seat cushion occurred. Vertical helmet displacement was always greater than eye displacement. The average difference was 0.47 cm, with little additional change occurring between 2.0 and 5.0 Gz. The data compare favorably with Kennedy (3) who reported up to 5.5 cm of eye displacement at 6.0 Gz. That study attributed 17% of the eye displacement to head pitch down and 83% to the slump of the subject.

-Gz Acceleration

The lap belt and shoulder harness restrains the crewmember against -Gz forces. The displacement is greater in this direction than in +Gz. Strap material, attachment geometry, tightness of adjustment, area of support, and other factors affect -Gz restraint. Our data were taken only at -1.0 Gz and resulted in an average upward vertical displacement of the eye of 4.79 cm. Lorch (5), using seven different restraint harness configurations, reported a displacement (helmet) range of 5 to 12 cm at -2.0 Gz. Leupp (4) reported buttock displacement off the seat pan of 3.6 cm at -2.0 Gz with human subjects. Off-seat displacement of 3.7 cm at -2.0 Gz and 6.4 cm at -5.0 Gz were also reported by Leupp when a 95 percentile manikin was used.

Gy Acceleration

Most aircraft are not capable of generating significant Gy (lateral) accelerations. Consequently, restraint systems are not designed to provide good lateral support. Mean eye displacement of 10.16 cm was recorded at 2.0 Gy (Table III). This is nearing the exit pupil of the typical HUD (12.7 cm). It was our observation that the subjects exposed to Gy acceleration experienced not only a lateral displacement but also bending of the torso or head-neck and rotation (primarily of the head). The data are for total sideward displacement and do not differentiate between displacement, bending, and rotation. Improving the standard restraint system by adding shoulder pad supports reduced, at the 2 Gy level, mean eye

displacement from 10.16 to 3.96 cm (61%) and shoulder displacement from 9.05 to 4.08 cm (55%). Increasing the Gz component decreased the force measured with an instrumented shoulder pad (Table II & Fig. 6) and probably reduced sideward displacement. It was the consensus of our subjects that the standard restraint system was inadequate above 1.5 Gy. Some of our subjects at 2.0 Gy experienced lateral head rotation estimated between 20° and 45°. This high degree of rotation in combination with the helmet and mask profile could obscure the viewing of some forward mounted cockpit instruments and be outside the viewing envelope of a HUD.

CONCLUSIONS

The stereoscopic photographic system was used on the DES to measure eye displacement during a variety of acceleration environments. Eye displacements of 3.95 cm have been measured at +4.0 Gz, 4.79 cm at -1.0 Gz, and 10.16 cm at 2.0 Gy. The system, once installed, is easy to use and non-invasive to the subject. The disadvantage of the system is that large amounts of data are time consuming to reduce. Our current plans are to replace the photographic system with a sonic digitizer system that will provide real time displacement data.

REFERENCES

1. Frazier JW, Repperger DW, Popplow JR, Rogers DB, O'Lear BA, and Gardner TR. The influence of Gy and Gz forces on biodynamic measurements. In: Preprints of the Aerospace Medical Association Annual Scientific Meeting. Washington DC: Aerospace Medical Association, 1982; 118-9.

2. Guthrie MA. Effects of Gz and Gy acceleration on head and helmet position displacement. Master Thesis, Wright State University, Dayton, Ohio, 1977.

3. Kennedy K, Kroemer KH. Excursions of head, helmet and helmet-attached reticle under +Gz forces. AMRL-TR-72-127 (AD-A767201), Aerospace Medical Research Laboratory, Wright-Patterson Air Force Base, Ohio, 1973.

4. Leapp D. Aces II negative Gz restraint investigation. AFAMRL-TR-83-049 (AD-A140326), Aerospace Medical Research Laboratory, Wright-Patterson Air Force Base, Ohio, 1983.

5. Lorch D. Centrifuge tests of modifications to the MA-2 aircrewman torso harness - phase 1. NADC-82126-60. U.S. Naval Air Development Center, Johnsville, PA, 1982.

6. Popplow JR, Veghte JH, Hudson KE. Cardiopulmonary responses to combined lateral and vertical acceleration. Aviat. Space Environ. Med. 1983; 54(7):632-6.

7. Repperger DW, Popplow JR, Rogers DB, Frazier JW, O'Lear BA, and Hudson KE. Performance effects resulting from a complex G experiment. In: Preprints of the Aerospace Medical Association Annual Scientific Meeting. Washington DC: Aerospace Medical Association, 1982; 77-8.

8. Stewart DF. The physiological and performance effects of sequential Gy/Gz accelerations. Master of Science Thesis, Department of Community Medicine, Wright State University, Dayton, Ohio, June 1983.

9. Van Patten RF, Repperger DW, Frazier JW. Pilot performance in sustained and oscillating lateral acceleration - AFTI/F-16 rudder tracking. AFAMRL-TR-82-85 (AD-A129802), Aerospace Medical Research Laboratory, Wright-Patterson Air Force Base, Ohio, 1982.

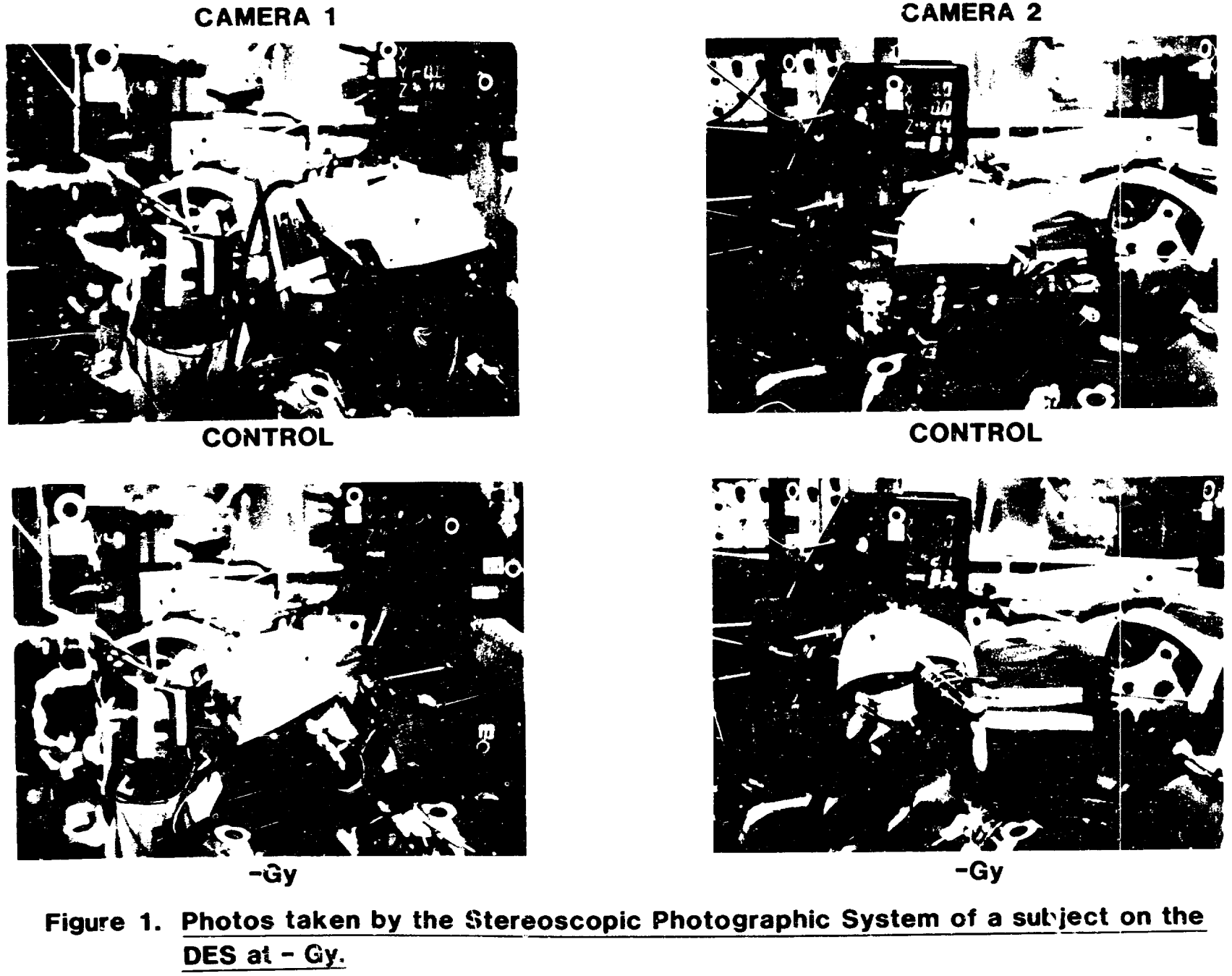

Figure 1. Photos taken by the Stereoscopic Photographic System of a subject on the DES at - Gy.

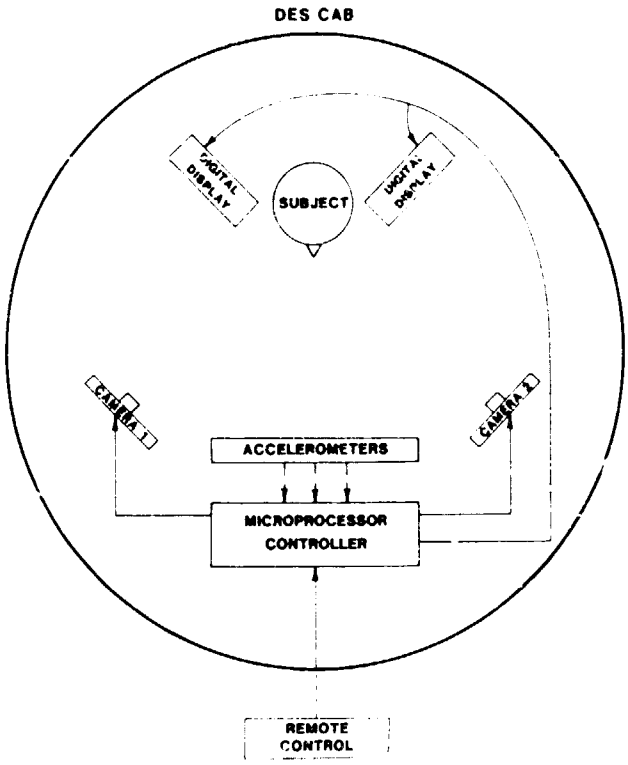

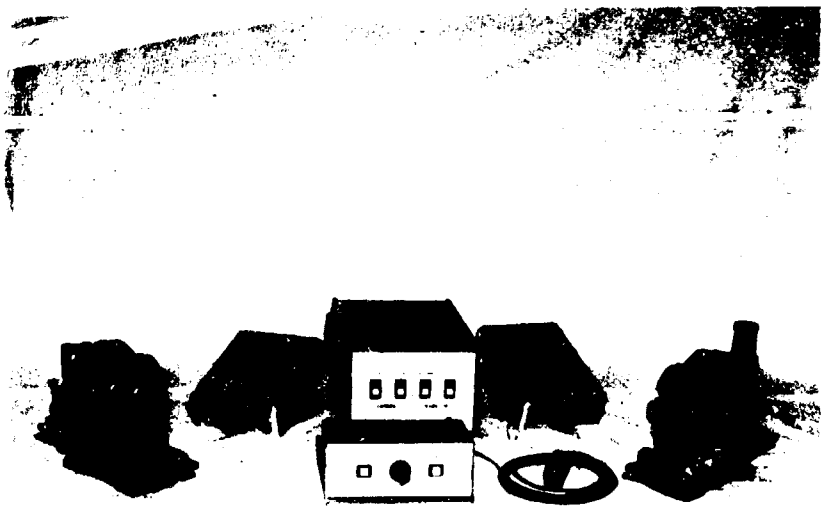

CAMERAS, CONTROLS, & DISPLAYS

Figure 2. Stereoscopic Photographic System.

Figure 3. Stencel Seat with Instrumented Shoulder Pad and Head Supports to measure +Gy restraining forces.

Figure 4. Subject at -2 Gy in the ACES II Seat.

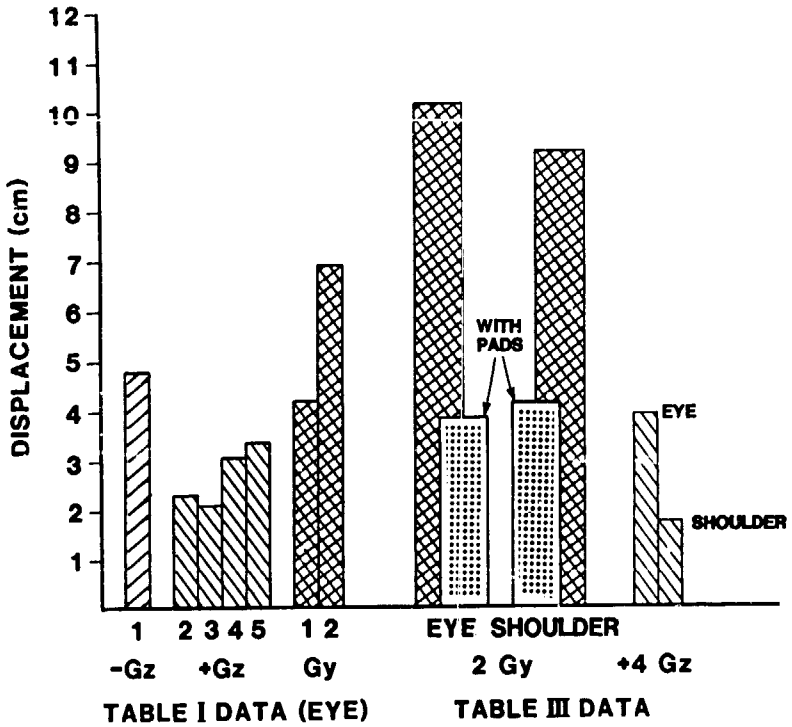

Figure 5. Displacements at various conditions.

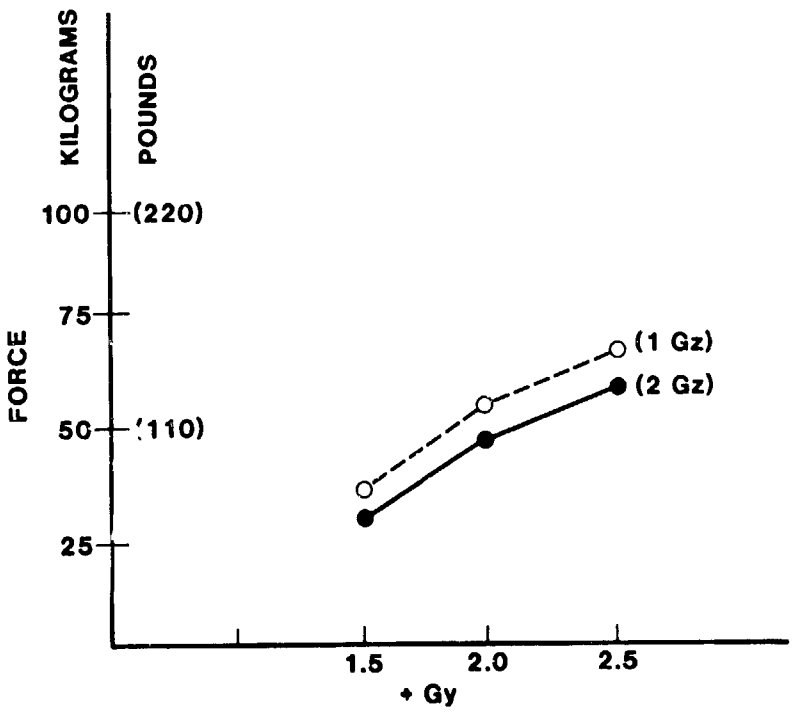

Figure 6. Left shoulder pad forces measured during sustained lateral G (TABLE III).

U.S. GOVERNMENT PRINTING OFFICE 1988 - 548-002/80201